Available online at www.sciencedirect.com

ScienceDirect

Procedia Structural Integrity 5 (2017) 239–246

Structural Integrity Procedia

www.elsevier.com/locate/procedia

2nd International Conference on Structural Integrity, ICSI 2017, 4-7 September 2017, Funchal, Madeira, Portugal

Analysis of fatigue crack propagation in laser sintering metal

L.F.P. Borrego[a,b]*, F.V. Antunes[a], J.A.M. Ferreira[a], J.D. Costa[a], C. Capela[a,c]

[a] *CEMMPRE, University of Coimbra, Department of Mechanical Engineering, Rua Luís Reis Santos, 3030-788, Coimbra, Portugal*
[b] *Instituto Politécnico de Coimbra, ISEC, Department of Mechanical Engineering,Rua Pedro Nunes, 3030-199 Coimbra, Portugal*
[c] *Instituto Politécnico de Leiria, Department of Mechanical Engineering, ESTGMorro do Lena – Alto Vieiro, 2400-901 Leiria, Portugal.*

Abstract

Laser sintering metal has recently been used in the manufacture of components for different applications like aerospace or medicine. The approach to engineering design based on the cracks propagation assumption applying the concepts of linear elastic fracture mechanics (LEFM) is commonly used for aerospace engineering. However, fatigue crack propagation is linked to irreversible and non-linear mechanisms at the crack tip, therefore LEFM parameters can be successfully replaced by non-linear crack parameters, namely the plastic CTOD. A model linking da/dN with plastic CTOD is proposed here to characterize fatigue crack propagation. A comparison is made with other materials showing that for the same plastic CTOD the laser sintering material has a relatively large crack growth rate.

Peer-review under responsibility of the Scientific Committee of ICSI 2017

Keywords: Laser sintering material; fatigue crack propagation; plastic CTOD

1. Introduction

Laser sintering metal (LSM) has recently been used in the manufacture of components for different applications like aerospace or medicine. Many studies, mainly focused on the influence of sintering parameters and selection of metal powder on microstructure of the sintered parts, state that for some materials, LSM parts are able to offer static mechanical properties comparable to the properties of conventionally bulk materials. However, on service the

* Corresponding author. Tel.: +351 962560101; fax: +351 239790331.
E-mail address: borrego@isec.pt

2452-3216
Peer-review under responsibility of the Scientific Committee of ICSI 2017
10.1016/j.prostr.2017.07.123

components are typically dynamically loaded, for which additional work is needed to fully understand the fatigue behavior and the relevant control parameters.

The analysis of fatigue crack propagation is usually conducted by relating the crack advance per unit cycle, da/dN, to the stress intensity factor range, ΔK. At intermediate values of ΔK, a power law relationship is generally observed. For long cracks, in the small-scale yielding range, the da/dN-ΔK relationship retains the advantage of Linear Elastic Fracture Mechanics (LEFM), namely the invariance relative to the shape and size of cracked solids. This linear-elastic parameter, surprisingly, was able to describe the rate of plastic processes at the crack tip. Later, Rice (1967) demonstrated that the small-scale cyclic plasticity at the crack tip was, indeed, controlled by ΔK. Nevertheless, da/dN-ΔK relations have several limitations, namely: (i) such curves are completely phenomenological, not derived from physics, and the fitting parameters have units with no physical justification; (ii) such curves are only valid in the small-scale yielding range; (iii) and da/dN depends on other parameters, including the stress ratio and the load history.

In order to overcome the difficulties related to the application of K to the analysis of fatigue crack growth (FCG), several concepts have been proposed. Crack closure (Elber, 1970) has been used to explain the effects of mean stress, overloads, short cracks and specimen thickness, while the T-stress has been used to explain the effect of specimen geometry (Lugo, 2011). Donald and Paris (1999) and Kujawski (2001) have introduced the concept of partial crack closure, so called, which recognizes that a significant contribution to fatigue damage occurs in the load range below the opening load as measured by the compliance technique. Closure, or interference of crack faces, only partially shields the crack tip from damaging action due to cyclic loading. Christopher *et al.* (2007) proposed a novel mathematical model based on the stresses around the crack tip, which has four parameters were used to characterize the stress field. However, these concepts only mitigated the problem and raised new issues.

In fact, fatigue crack growth is caused by crack tip plastic deformation, therefore ΔK parameter must be replaced by a non-linear crack tip parameter. The non-linear parameters identified in the literature review made by Antunes *et al.* (2015) were the range of cyclic plastic strain, the size of reversed plastic zone, the total plastic dissipation per cycle and the crack opening displacement. The crack opening displacement (COD) is a classical parameter in elastic-plastic fracture mechanics, still widely used nowadays. It has a physical meaning and can be measured directly in experiments. In the finite element analysis, the displacement of the first node behind the crack tip is generally used as an operational crack tip opening displacement (CTOD). The capabilities of CTOD to study crack closure and fatigue crack growth were fully demonstrated in previous work of the authors (Antunes, 2017).

The main purpose of the present work is to define a da/dN versus plastic CTOD relation for the laser sintering AISI 18Ni300 maraging steel. Fatigue crack propagation, da/dN, was obtained and afterwards a numerical study was defined, replicating the experimental procedure in order to obtain the plastic CTOD. The numerical model intended to be realistic in terms of geometry of the specimen and crack, in terms of loading and in terms of material behavior. The accurate modeling of material hardening is of major importance for the quality of numerical predictions. The behavior of the material was obtained from low-cycle fatigue experimental tests with smooth specimens tested under constant amplitude strain range. The stress-strain loops were used for the analytical fitting of hardening models. Finally, the da/dN versus plastic CTOD model was used to predict fatigue crack propagation for load blocks. The development of da/dN versus plastic CTOD relations is based on two basic assumptions: (i) that fatigue crack growth is intimately linked to crack tip plastic deformation. (ii) that the CTOD is able to quantify the plastic deformation occurring at the crack tip.

2. Experimental fatigue crack growth

Fatigue crack growth tests were carried out at room temperature using a 10 kN capacity Instron Electropuls E10000 machine, with a frequency within the range 15–20 Hz. conducted following the recommendations outlined in ASTM E647 standard using C(T) specimens (see Figure 1a). Specimens were produced by laser sintering with a thickness of 3 mm. The final surface finishing was achieved by high-speed mechanical polishing.

The crack length was measured from a travelling microscope, with magnification of 45x, and with an accuracy of 10 μm. The five-point incremental polynomial method was used to obtain the fatigue crack growth rates (FCGR). The applied loads were P_{max}=1488.4 N and P_{min}=74.4 N, therefore with a stress ratio R=0.05. Figure 1b shows da/dN versus ΔK results in log-log scales.

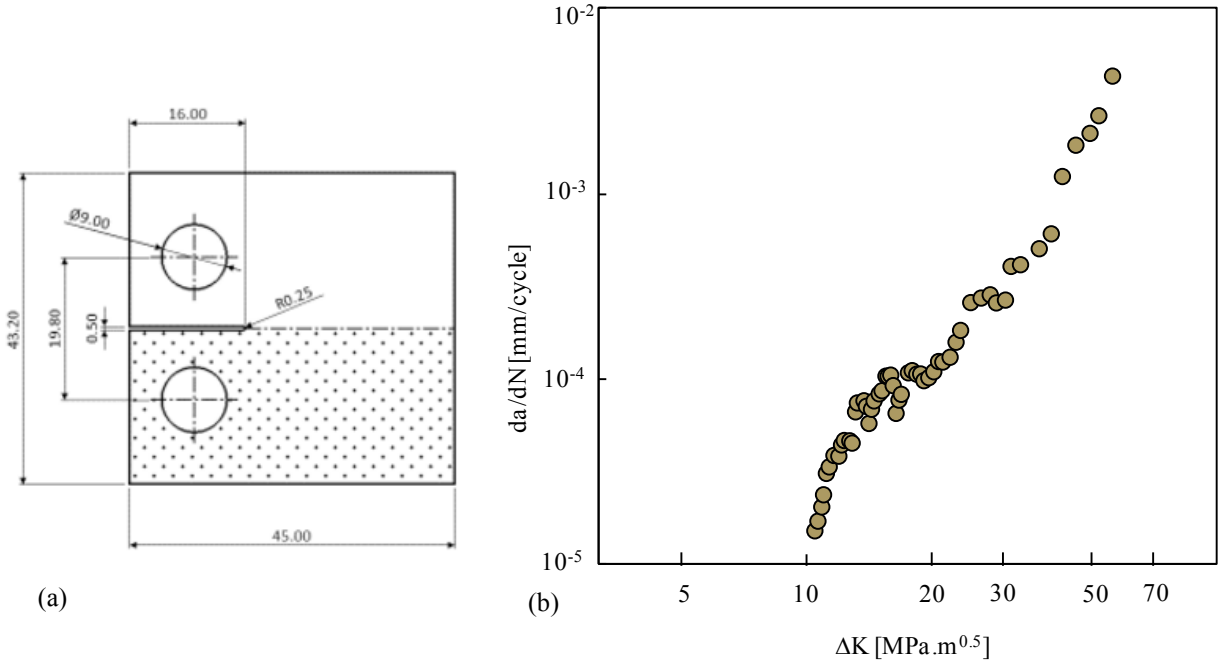

Fig. 1. (a) Geometry of CT specimen. (b) da/dN-ΔK plot in log-log scales.

3. Model to characterize the cyclic plastic deformation

3.1. Low cycle fatigue tests

Low-cycle fatigue tests were conducted on a DARTEC servo-hydraulic testing machine, equipped with a 100 kN load cell, at room temperature, and in laboratory air environment. The tests were conducted under axial total strain-controlled mode, with sinusoidal waves, using a constant strain rate (da/dt) equal to 0.008 s-1, and total strain ratios (Rε) of -1 and total strain amplitude (Δε/2) equal to 0.8%. Specimens were precisely produced according to the specifications outlined in ASTM E606 with a gage section measuring 25 mm in length and 6 mm in diameter specimens. The final surface finishing was obtained by high-speed mechanical polishing using different grades of silicon carbide papers (P600-grit, P1200-grit, and P2500-grit) followed by 3-μm diamond paste. A 12.5-mm strain-gage extensometer was attached directly to the specimen gage section, using rubber bands, to evaluate the stress-strain relationship throughout the test. For each loading cycle, 200 samples were collected using a PC-based acquisition system. Figure 2 shows the stress-strain curve obtained. As can be noted, the material response is nearly stable.

3.2. Fitting of material constants

High precision in the numerical results generated by FEM, namely those of plastic CTOD, depends on the accurate modeling of the material elastic-plastic behavior. The elastic-plastic model adopted in this work assumes: (i) the isotropic elastic behavior modeled by the generalized Hooke's law (the values of the elastic constants are shown in Table 2); (ii) the plastic behavior follows the von Mises yield criterion, coupled with Voce isotropic hardening law and Lemaître-Chaboche non-linear kinematic hardening law, under an associated flow rule. The von Mises yield surface is described by the equation:

$$\left(\Sigma_{22}-\Sigma_{33}\right)^2+\left(\Sigma_{33}-\Sigma_{11}\right)^2+\left(\Sigma_{11}-\Sigma_{22}\right)^2+3\Sigma_{23}^2+3\Sigma_{13}^2+3\Sigma_{12}^2=2Y^2 \tag{1}$$

where Σ_{11}, Σ_{22}, Σ_{33}, Σ_{12}, Σ_{13}, and Σ_{23} are the components of the effective stress tensor, Σ ($\Sigma = \sigma' - X$, where σ' is the deviatoric component of the Cauchy stress tensor and X is the backstress tensor); Y is the yield stress, and its evolution with plastic strain is modeled by the Voce hardening law:

$$Y(\bar{\varepsilon}^{\mathrm{p}})=Y_0+(Y_{\mathrm{Sat}}-Y_0)[1-\exp(-C_{\mathrm{Y}}\bar{\varepsilon}^{\mathrm{p}})] \tag{2}$$

where Y_0, Y_{Sat} and C_{Y} are material parameters and $\bar{\varepsilon}^{\mathrm{p}}$ is the equivalent plastic strain. The Lemaître-Chaboche kinematic hardening law is:

$$\dot{\mathbf{X}}=C_{\mathrm{X}}\left[X_{\mathrm{Sat}}\frac{\boldsymbol{\sigma}'-\mathbf{X}}{\bar{\sigma}}-\mathbf{X}\right]\dot{\bar{\varepsilon}}^{\mathrm{p}} \tag{3}$$

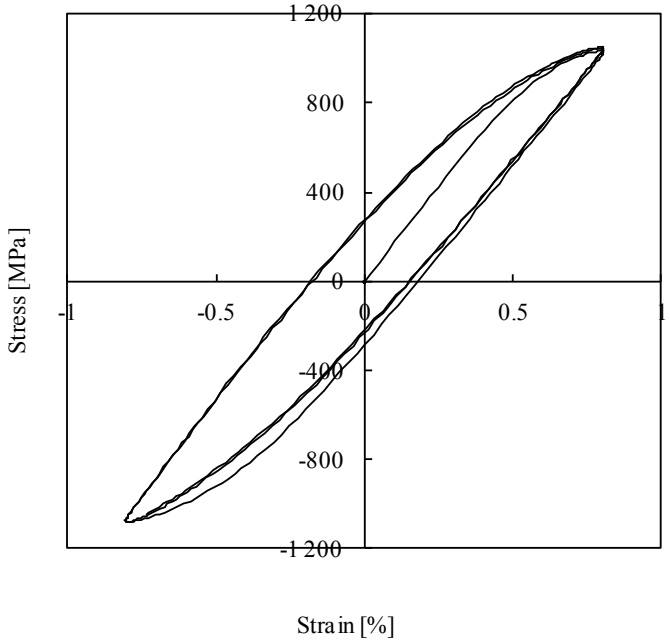

Fig. 2. Stress-strain plot (Δε=±0.8%).

where C_{X} and X_{Sat} are material parameters and $\dot{\bar{\varepsilon}}^{\mathrm{p}}$ is the equivalent plastic strain rate. The identification of the material parameters that best describe the plastic behaviour of AA7050-T6 was carried out by minimizing the cost function F(A):

$$F(\mathbf{A})=\sum_{i=1}^{N}\left(\frac{\sigma^{\mathrm{Fit}}(\mathbf{A})-\sigma^{\mathrm{Exp}}}{\sigma^{\mathrm{Exp}}}\right)_i^2 \tag{4}$$

where $\sigma^{\mathrm{Fit}}(\mathbf{A})$ and σ^{Exp} are the fitted and the experimentally measured values of true stress, respectively; A is the set of Voce and Lemaitre-Chaboche parameters that minimises F(A); N is the total number of experimental points.

The values of σ^{Exp} were obtained from the low-cycle fatigue test. The fitting was performed using the Microsoft Excel SOLVER tool, which resorts to the Generalised Reduced Gradient (GRG2) non-linear optimization algorithm. Table 1 shows the material constants obtained.

Table 1. Identified parameter values.

An example of a column heading	Voce law parameters			Lemaître-Chaboche law parameters	
	Y_0 [MPa]	Y_{Sat} [MPa]	C_Y	C_X	X_{Sat} [MPa]
Identified values	894.3	894.3	0.0001	969.24	194.9

4. Numerical determination of plastic CTOD

4.1. Numerical model

The geometry of the CT specimens was presented in Figure 1a. Since this geometry is symmetric relatively to one plane in terms of geometry, material and loading, only 1/2 of the specimen was modeled numerically, considering proper boundary conditions. A small thickness of 0.1 mm was assumed in order to simulate pure plane stress state. Different initial crack lengths were assumed, a_0=7, 10, 13, 16, 19, 22 and 24 mm, in order to replicate different experimental crack lengths. The maximum and minimum remote loads were kept constant with values of 49.6 and 2.48 N, respectively.

The finite element mesh comprised 7175 linear isoparametric elements and 14678 nodes. It has two main regions: an ultra-refined rectangular box, near the crack tip, created with elements of 8×8 μm side; and a coarser mesh in the remaining volume of the body in order to reduce the computational overhead. In the thickness direction, only one layer of elements was used. The crack propagated uniformly over the thickness, at the minimum load, by successive debonding of both crack front nodes. A total of 159 crack propagations were modeled, corresponding to a crack advance (Δa) of 1272 μm (i.e., Δa = (160-1)×8 μm). Between each crack increment, which corresponds to one finite element, were applied five load cycles. The symbol NLC indicates the number of load cycles between crack increments.

The three-dimensional finite element software used to implement the numerical model was the DD3IMP in-house code. This implicit FE code was originally developed to model deep drawing (Oliveira, 2008), therefore has a great competence in the prediction of plastic deformation. The evolution of the deformation process is described by an updated Lagrangian scheme, assuming a hypoelastic-plastic model. Thus, the mechanical model takes into account large elastoplastic strains and rotations and assumes that the elastic strains are negligibly small with respect to unity. The plastic behavior is modeled considering the set of material parameters shown in Table 1. The contact of the crack flanks is modeled considering a rigid body (plane surface) aligned with the crack symmetry plane. A master–slave algorithm is adopted and the contact problem is treated using an augmented Lagrangian approach. The CTOD was typically measured at the first node behind crack tip, i.e., at a distance of 8 μm from crack tip.

4.2. Numerical results

Figure 3 presents typical results of CTOD versus remote stress, obtained for an initial crack length a=24.16 mm. Five load cycles were applied between each crack increment and the CTOD was measured at the first node behind crack tip, as is schematically indicated in Figure 3. For relatively low loads, between A and B, the crack is closed, i.e., the CTOD is zero. The increase of the load opens the crack at point B. After point B, the crack opens linearly with load increase, up to point C, which is the boundary of the elastic regime. Between points C and D, there is a progressive increase of plastic deformation, which has its maximum value for the maximum load. The decrease of the load produces reversed elastic deformation with the same rate observed during loading. The posterior decrease of load

produces reversed plastic deformation. The variation of plastic CTOD is also plotted in Figure 3. Plastic deformation starts at point C and has its maximum value at maximum load. Fatigue crack propagation is correlated in here with the range of plastic CTOD, $\Delta CTOD_p$, indicated in figure 3. Note that crack closure is naturally included in the value of $\Delta CTODp$. The increase of crack closure phenomenon reduces the effective range of stress, reducing the total CTOD and the plastic CTOD. In the absence of crack closure, all load cycle is felt by the crack tip. The plastic CTOD also does not consider the elastic deformation, which in fact is not supposed to affect FCG.

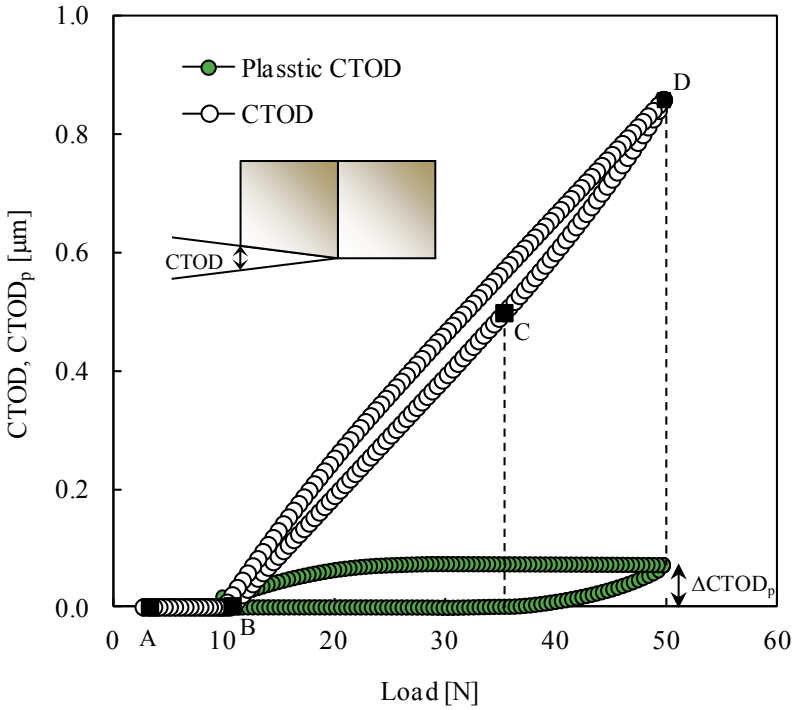

Fig. 3. Variation of CTOD with load (a_0=24 mm).

Figure 4 presents plastic CTOD range versus da/dN for different crack length. As can be seen there is a progressive increase of FCGR with plastic $\Delta CTOD_p$. The values of $\Delta CTOD_p$ are relatively small. A model was fitted to these results:

$$\frac{da}{dN} = 231577 \times \Delta CTOD_p^4 - 22802 \times \Delta CTOD_p^3 + 716.13 \times \Delta CTOD_p^2 - 0.6473 \times \Delta CTOD_p \quad (5)$$

where the units of da/dN and $\Delta CTOD_p$ are μm/cycle and μm, respectively. Results for two other materials are also presented in Figure 4. As can be seen, for the same $\Delta CTOD_p$, the fatigue crack growth rate is significantly higher for the laser sintered material (LSM) comparatively with the 6082-T6 and 7050-T6 aluminium alloys.

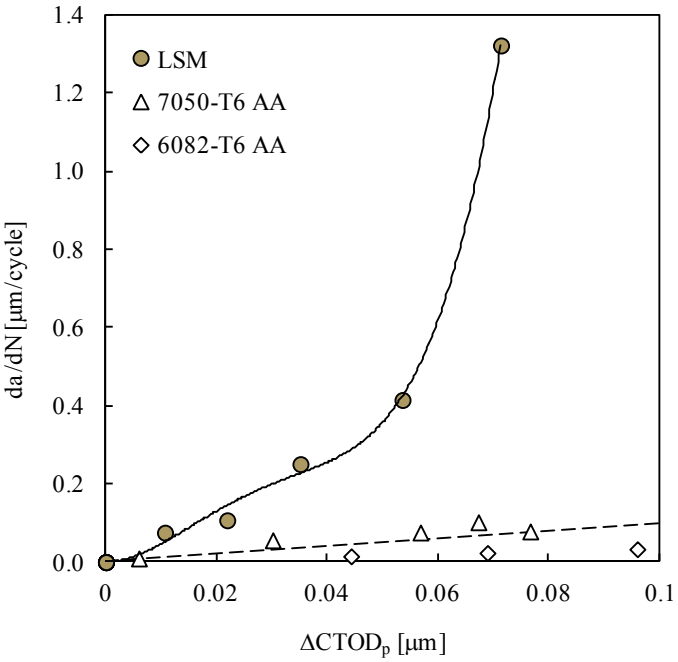

Fig. 4. FCGR versus plastic CTOD.

5. Conclusions

Fatigue crack propagation in the laser sintering AISI 18Ni300 maraging steel was studied using a da/dN versus plastic CTOD relation. Fatigue crack growth rate, da/dN, was determined experimentally in CT specimens with 3 mm of thickness. The plastic CTOD range, $\Delta CTOD_p$, was predicted numerically using the finite element method. The numerical model replicated the experimental procedure in terms of geometry, loading and material properties. The analytical model of the elastic-plastic behaviour was based on cyclic stress-strain curves obtained in smooth specimens. A well defined relation was found between $\Delta CTOD_p$ and da/dN, which is non linear. The comparison with other materials showed that, for the same plastic CTOD, the relatively high for the laser sintered material.

Acknowledgements

The authors would like to acknowledge the sponsoring under the project number 016713 (PTDC/EMS-PRO/1356/2014) financed by Project 3599 Promover a Produção Científica e Desenvolvimento Tecnológico e a Constituição de Redes Temáticas (3599-PPCDT) and FEDER funds and also EROFIO S.A. industry for the supply of the testing samples.

References

Rice, J.R., 1967. Mechanics of crack tip deformation and extension by fatigue. In: Fatigue crack propagation. Philadelphia: ASTM STP 415, 256–271.

Elber, W., 1970. Fatigue crack closure under cyclic tension. Engineering Fracture Mechanics 2, 37-45.

Lugo, M. and Daniewicz, S.R., 2011. The influence of T-stress on plasticity induced crack closure under plane strain conditions. International Journal of Fatigue 33, 176–185.

Donald, K., Paris, P.C., 1999. An evaluation of ΔK_{eff} estimation procedure on 6061-T6 and 2024-T3 aluminum alloys. International Journal of Fatigue 21, S47–57.

Kujawski, D., 2001. Enhanced model of partial crack closure for correlation of R-ratio effects in aluminum alloys. International Journal of Fatigue 23, 95–102.

Christopher, C.J., James, M.N., Patterson, E.A. and Tee, K.F., 2007. Towards a new model of crack tip stress fields, International Journal of Fracture 148, 361–371.

Antunes, F.V., Sousa, T., Branco, R., Correia, L., 2015. Effect of crack closure on non-linear crack tip parameters. International Journal of Fatigue 71, 53–63.

F.V. Antunes, R Branco, P.A. Prates, L. Borrego, 2017. Fatigue crack growth modelling based on CTOD for the 7050-T6 alloy, Fatigue Fract Engng Mater Struct (in press).

Oliveira, M.C., Alves, J.L. Menezes, L.F., 2008. Algorithms and Strategies for Treatment of Large Deformation Frictional Contact in the Numerical Simulation of Deep Drawing Process. Archives of Computational Methods in Engineering 15, 113-162.